Colloidal stabilization via nanoparticle halo formation

Jiwen Liu and Erik Luijten*

*Department of Materials Science and Engineering and Frederick Seitz Materials Research Laboratory,
University of Illinois at Urbana-Champaign, Urbana, Illinois 61801, USA*
(Received 30 July 2005; published 6 December 2005)

We present a detailed numerical study of effective interactions between micrometer-sized silica spheres, induced by highly charged zirconia nanoparticles. It is demonstrated that the effective interactions are consistent with a recently discovered mechanism for colloidal stabilization. In accordance with the experimental observations, small nanoparticle concentrations induce an effective repulsion that counteracts the intrinsic van der Waals attraction between the colloids and thus stabilizes the suspension. At higher nanoparticle concentrations an attractive potential is recovered, resulting in reentrant gelation. Monte Carlo simulations of this highly size-asymmetric mixture are made possible by means of a geometric cluster Monte Carlo algorithm. A comparison is made to results obtained from the Ornstein-Zernike equations with the hypernetted-chain closure.

I. INTRODUCTION

Colloidal suspensions are used in a wide range of applications, such as coatings and drug carriers, and as a precursor for various advanced materials, including colloidal crystals. In all these systems, the *stability* of the suspension plays a central role. The van der Waals attractions between the colloids—if not counteracted by some appropriate mechanism—lead to their aggregation, typically resulting in the formation of a gel. Conventional methods to mitigate the effect of the van der Waals forces rely on charge stabilization or steric stabilization [1]. In charge stabilization, an electrostatic repulsion between the colloids is induced, e.g., by an appropriate choice of the *p*H. Steric stabilization frequently involves grafting short polymer chains onto the colloidal surface, which prevents a close approach of the colloidal surfaces.

Quite recently, an alternative strategy for colloidal stabilization has been discovered [2]. These experiments involve an aqueous suspension of silica spheres with a diameter $\sigma_{\rm micro}$ of approximately 0.6 μm, to which charged zirconia nanoparticles of much smaller diameter ($\sigma_{\rm nano}=6$ nm) are added. In the absence of nanoparticles, as well as in the presence of very small concentrations of nanoparticles, the microspheres exhibit a tendency to aggregate owing to their van der Waals attraction. Increasing the nanoparticle concentration *prevents* this aggregation and thus stabilizes the suspension. At even higher zirconia concentrations, the aggregation behavior reappears, leading to a "window of stability" in the nanoparticle concentration. In order to ensure that the observed stability does not result from direct electrostatic repulsion between the microspheres, the suspension is kept at a very low *p*H, near the isoelectric point of silica. Furthermore, it has been verified in Ref. [2] that there is no strong adsorption of nanoparticles on the silica surface, which would lead to an effective surface charge accumulation on the colloids and thus again would result in electrostatic sta-

bilization. Specifically, the amount of zirconia associated with the microspheres was determined from supernatant measurements employing inductively coupled plasma analysis (indicating weak adsorption) as well as from scanning angle reflectometry of a silica surface immersed in the nanoparticle solution (indicating no detectable adsorption at all). We view the former analysis as more representative, since it involves the actual silica microspheres for which the reported phase behavior was determined.

Since there are only very few approaches for the stabilization of colloidal suspensions, it is of clear importance to explore the underlying mechanism of these observations. Not only may a new stabilization technique be of practical significance, the binary mixture investigated in Ref. [2] also constitutes an interesting model system for the exploration of depletion effects [3] in nonadditive systems [4–6]. Lewis and co-workers [2] ascribe the initial colloidal stabilization to the formation of a "halo" of zirconia particles around the silica colloids, arising from the strong electrostatic repulsion between nanoparticles. However, while consistent with ζ-potential measurements that confirm a weak accumulation of nanoparticles near the colloidal surface [2], such halo formation is at variance with the observation of stabilization at zirconia volume fractions below 10^{-3}, where the average nanoparticle separation greatly exceeds the electrostatic screening length λ. Indeed, a rather high concentration of nitric acid is required to reach the isoelectric point of silica, resulting in $\lambda \approx 2$ nm [7], only one-third of the nanoparticle diameter. On the other hand, explanation of the reentrant gelation representing the upper boundary of the stability window appears more straightforward and is attributed in Ref. [2] to the regular depletion attraction [3] induced by the nanoparticles. While this can not be excluded *a priori*, it must be noted that nonadditivity effects can significantly alter the nature of the depletion interaction [8].

In Ref. [9] we have studied this system by means of canonical Monte Carlo simulations. While particle-based simulations can explicitly account for the fluctuation and correlation effects that are ignored in many analytical methods, it is important to note that the extreme size asymmetry $\alpha = \sigma_{\rm micro}/\sigma_{\rm nano} = 100$ places the current system out of reach for

---

*Corresponding author. Email address: luijten@uiuc.edu

conventional Monte Carlo and molecular dynamics simulations. This was resolved by means of a novel, highly efficient Monte Carlo scheme [10–12] that is capable of simultaneously equilibrating interacting species of vastly different sizes. In this article, we present a detailed technical account of the calculations reported in Ref. [9] and make a comparison with results obtained in an integral-equation study of the same system [13–15].

Understanding and prediction of phase behavior and stability of a suspension relies on a fundamental knowledge of the *effective* forces between colloids [16], which arise from a combination of direct interactions and indirect interactions mediated through the solvent and through other solute particles. It is this potential of mean force that we determine in the simulations, as a function of nanoparticle concentration. Our findings confirm the experimental observations on a quantitative level and, in combination with the corresponding nanoparticle distributions, clarify the physical mechanism of the stabilization. Consequently, our computational approach also has predictive capabilities, allowing the stability window to be tuned as a function of nanoparticle charge and microsphere–nanoparticle size asymmetry.

II. COLLOID–NANOPARTICLE INTERACTIONS

It is the purpose of our calculation to determine the effective interaction $V_{\text{micro}}^{\text{eff}}(r)$ between a pair of colloidal microspheres induced by the nanoparticles. Calculation of $V_{\text{micro}}^{\text{eff}}(r)$ amounts to integrating out the degrees of freedom of the nanoparticles in the partition function [17,18],

$$e^{-\beta[V_{\text{micro}}^{\text{eff}}(r)+V_{\text{micro}}(r)]} = \sum_{\{s_{\text{nano}}\}} e^{-\beta\mathcal{H}(r;\{\mathbf{r}\})}, \qquad (1)$$

where $\mathcal{H}(r;\{\mathbf{r}\})$ is the Hamiltonian describing a system containing two microspheres at a separation r and a set of nanoparticles with coordinates $\{\mathbf{r}\}$. $V_{\text{micro}}(r)$ represents the direct microsphere pair potential and β indicates the inverse temperature $(k_BT)^{-1}$, with k_B Boltzmann's constant and T the absolute temperature. The sum runs over all nanoparticle configurations s_{nano}. In order to avoid colloidal many-body effects, the infinite dilution limit must be taken for the microspheres. The required direct interactions between nanoparticles and between nanoparticles and microspheres are modeled as pairwise potentials $V_{\text{nano}}(r)$ and $V_{\text{m-n}}(r)$, respectively. Thus, the Hamiltonian can be written as

$$\mathcal{H}(r;\{\mathbf{r}\}) = V_{\text{micro}}(r) + \sum_{i,j\in\{\text{nano}\}} V_{\text{nano}}(|\mathbf{r}_{ij}|)$$
$$+ \sum_{i,j\in\{\text{m-n}\}} V_{\text{m-n}}(|\mathbf{r}_{ij}|), \qquad (2)$$

where the first sum runs over all pairs of nanoparticles, the second sum runs over all pairs consisting of a microsphere and a nanoparticle, and $\mathbf{r}_{ij} \equiv \mathbf{r}_j - \mathbf{r}_i$ indicates the pair separation. Since $V_{\text{micro}}(r)$ factorizes in Eq. (1), the nanoparticle-induced pair potential is independent of the direct microsphere interaction.

In our simulation, both colloidal microspheres and nanoparticles are modeled as hard spheres with diameters σ_{micro}

and σ_{nano}, respectively. We approximate the electrostatic double-layer interactions V_{nano} and $V_{\text{m-n}}$ via an extension of the Derjaguin-Landau-Verwey-Overbeek (DLVO) theory [19] to nonidentical particles. The Debye-Hückel approximation is used to linearize the Poisson-Boltzmann equation. Subsequent application of the Derjaguin approximation then leads to the Hogg-Healy-Fuerstenau (HHF) equation [20]. For a pair of particles at surface-to-surface distance D, under the condition of constant surface potential, this equation is given by

$$V_{\text{HHF}}(D) = \frac{1}{2}\varepsilon_0\varepsilon_r\pi\frac{\sigma_1\sigma_2}{\sigma_1+\sigma_2}(\Psi_1^2+\Psi_2^2)$$
$$\times\left[\frac{2\Psi_1\Psi_2}{\Psi_1^2+\Psi_2^2}\ln\left(\frac{1+\exp(-\kappa D)}{1-\exp(-\kappa D)}\right)\right.$$
$$\left.+\ln[1-\exp(-2\kappa D)]\right], \qquad (3)$$

where Ψ_i and σ_i ($i=1, 2$) represent the surface potential and diameter, respectively, of a particle of species i, ε_0 denotes the vacuum permittivity, $\varepsilon_r=80$ is the dielectric constant of water, and κ is the inverse of the Debye length.

For the interaction between two zirconia nanoparticles, $\Psi_1=\Psi_2=\Psi_{\text{nano}}$ and $\sigma_1=\sigma_2=\sigma_{\text{nano}}$, and Eq. (3) reduces to ([1], Chap. 12)

$$V_{\text{nano}}(D) = \varepsilon_0\varepsilon_r\pi\sigma_{\text{nano}}\Psi_{\text{nano}}^2\ln[1+\exp(-\kappa D)]. \qquad (4)$$

Due to the strong screening conditions in Ref. [2], we can invoke the approximation $\kappa D \gg 1$ to further simplify this expression to

$$V_{\text{nano}}(D) = \varepsilon_0\varepsilon_r\pi\sigma_{\text{nano}}\Psi_{\text{nano}}^2\exp(-\kappa D). \qquad (5)$$

While this last approximation overestimates the potential for $\kappa D \lesssim 1$, i.e., for $D \lesssim \kappa^{-1}=2$ nm, we note that at such small distances even the validity of the original expression Eq. (4) becomes less certain. Furthermore, at these distances hydration forces become important. As the hydration forces have a range of 1–2 nm and decay exponentially with a very short decay length [21], we account for the hydration shell of the zirconia particles by replacing σ_{nano} with $\sigma'_{\text{nano}}=\sigma_{\text{nano}}+1.5$ nm *solely* in Eq. (5).

Since, under the experimental conditions of Ref. [2], the silica microspheres are near their isoelectric point and thus have $\Psi_{\text{micro}}=0$, we ignore the electrostatic interaction between silica particles. However, Eq. (3) shows that an electrostatic double-layer interaction can arise between the microspheres and the nanoparticles, even though the former are neutral. For large size asymmetry $\alpha \equiv \sigma_{\text{micro}}/\sigma_{\text{nano}} \gg 1$, Eq. (3) reduces to

$$V_{\text{m-n}}(D) = \frac{1}{2}\varepsilon_0\varepsilon_r\pi\sigma_{\text{nano}}\Psi_{\text{nano}}^2\ln[1-\exp(-2\kappa D)], \quad (6)$$

which under the approximation $\kappa D \gg 1$ can be further reduced to

$$V_{\text{m-n}}(D) = -\frac{1}{2}\varepsilon_0\varepsilon_r\pi\sigma_{\text{nano}}\Psi_{\text{nano}}^2\exp(-2\kappa D). \qquad (7)$$

The presence of an electrostatic attraction may appear to contradict well-known results from Poisson–Boltzmann theory [22]. However, under *constant-potential* conditions a weakly charged particle near a strongly charged particle can acquire an opposite charge due to image-charge effects, resulting in an electrostatic attraction.

Three important approximations have been made in the derivation of the HHF equation. First, the linearized Poisson–Boltzmann theory following from the Debye-Hückel approximation is appropriate only for low surface potentials. For moderate to high surface potentials, Ψ_i ($i=1,\ 2$) in Eq. (3) has to be replaced by an effective surface potential $Y_i(D) = 4(\Psi_i/y_i^s)\exp(\kappa D/2)\tanh^{-1}[\exp(-\kappa D/2)\tanh(y_i^s/4)]$ with $y_i^s = e\Psi_i/k_B T$ [1,23]. As a result, the HHF equation overestimates the electrostatic interactions for the experimental value $\Psi_{\text{nano}}=70$ mV by up to 25% at large separations. For small values of κD, the effect is considerably less (cf. Fig. 2 in Ref. [23]). Second, the application of the Derjaguin approximation makes the HHF equation valid only for small κD. However, a strict derivation [23] without this approximation shows that the HHF formula can be rendered applicable to all κD by replacing $(\sigma_1\sigma_2)/(\sigma_1+\sigma_2)$ with $(\sigma_1\sigma_2)/(\sigma_1+\sigma_2+2D)$. For the short separations and large size ratio investigated here, the difference between these factors becomes negligible. Thirdly, a constant surface potential is assumed in Eq. (3), although charge-regulating boundary conditions are more appropriate for the oxide particles employed in Ref. [2]. However, both conditions have been found to lead to comparable results [24,25], in which an attraction can arise between neutral and charged surfaces, although it must be noted that there can be various, essentially different, physical origins of this attraction [24,26]. The attraction found in Ref. [24] arises from ion-ion correlations ignored in mean-field theory, whereas at constant surface potential the attraction arises from the image-charge effect in which ions are exchanged between the double layers of charged nanoparticles and neutral microspheres. It is important to emphasize that the mean-field approach of Ref. [20] is employed only to set up the direct colloid-nanoparticle and nanoparticle-nanoparticle *pair potentials* to be employed in the Monte Carlo simulations. The actual simulations explicitly take into account correlation and fluctuation effects for the nanoparticles. In addition, as is clear from the use of the HHF equation, the solvent and all ions are modeled implicitly, yielding a dielectric medium with a specific electrostatic screening length. While the sheer number of solvent molecules and ions precludes their explicit incorporation in the calculation, the strong screening also renders this largely unnecessary. Another noteworthy point is that the calculations presented here only yield the effective colloidal pair potential. Triplet and higher-order interactions, which may become important under the nondilute conditions in the experiments, are not addressed.

The presence of an attractive interaction between microspheres and nanoparticles, as found in Eq. (7), is consistent with the supernatant measurements reported by Tohver *et al.* [2]. Also their ζ-potential measurements [2] (which exploit the electrophoretic mobility of the microspheres) indicate a certain degree of microsphere-nanoparticle association, since the increase of the zeta potential with increasing nanoparticle concentration requires a cooperative motion of colloids and nanoparticles. Accordingly, it might be tempting to dismiss the haloing phenomenon as a standard case of electrostatic stabilization resulting from an effective charge buildup on the colloids. However, as is shown below, the situation is considerably more complicated, since the resulting halo is dynamic in nature and leads to effective interactions that are attractive, repulsive, or oscillatory, depending on nanoparticle concentration.

III. SIMULATION DETAILS

As already noted in Ref. [11], traditional computational approaches experience severe difficulties in the treatment of this system. Inherent limitations in most computational methodologies greatly restrict the range of accessible size ratios in multicomponent mixtures because larger species tend to get trapped by the smaller. This ergodicity problem becomes more severe if small particles accumulate around larger ones, as is the case in the present system [2,7]. The simulation methods that are capable of explicitly simulating both large and small species are limited to size ratios up to $\alpha=10$ [27], except for a few cases of hard-sphere mixtures. Thus, an alternative route that is sometimes taken is to only simulate the smaller species around a pair of immobile large particles at a fixed separation [28–30]. Since the effective force can be evaluated only for one separation at a time, a series of such simulations for different large-particle distances must be carried out to construct the entire curve for the effective force. Since the large-particle concentration must be kept very small to exclude many-body effects, the total particle number typically becomes very large if the small species is present at a fixed concentration and α is large. As a result, this method becomes impractically slow even for moderate accuracy.

We overcome this problem by exploiting a highly efficient Monte Carlo scheme [11,12], which permits the explicit inclusion of interacting species of vastly different sizes. This algorithm is a variant of the geometric cluster algorithm originally introduced by Dress and Krauth [10]. The explicit simulation of both species makes it possible to calculate the effective interactions directly from the inversion of the particle pair correlation function $g(r)$ with less computational effort than previous techniques. In the infinite dilution limit, the potential of mean force follows from $V_{\text{eff}}(r) = -k_B T \ln g(r)$. We employ only two microspheres in a periodic cubic box with linear length $L \approx 806\sigma_{\text{nano}}$ at concentration $\phi_{\text{micro}}=0.002$. In principle, the potential of mean force must be calculated from simulations in which the nanoparticles are kept at constant chemical potential. For efficiency reasons, we instead use the canonical ensemble, in which the number of nanoparticles is constant. Since our simulation cell is very large, fluctuations in the number of nanoparticles are expected to be small as the microsphere separation var-

TABLE I. Computational parameters for the various nanoparticle concentrations ϕ_{nano} investigated. All data apply to a nanoparticle-microsphere mixture containing two microspheres at a volume fraction ϕ_{micro} =0.002, with a colloid-nanoparticle size ratio α=100. N_{nano} indicates the number of nanoparticles in the simulation cell. $\langle N_{micro}^{cluster} \rangle$ and $\langle N_{nano}^{cluster} \rangle$ indicate the average number of microspheres and nanoparticles, respectively, in each cluster. Note that each cluster is started from a microsphere. Also shown are the total number of clusters constructed and the required CPU time.

ϕ_{nano}	N_{nano}	$\langle N_{micro}^{cluster} \rangle$	$\langle N_{nano}^{cluster} \rangle$	No. of clusters	CPU hours
0.0007	700 000	1.0089	2503	200 000 000	1,000
0.0010	1 000 000	1.0089	2626	200 000 000	1,800
0.0030	3 000 000	1.0092	5791	50 000 000	1,500
0.0050	5 000 000	1.0098	8737	40 000 000	3,100
0.0070	7 000 000	1.0110	11808	60 000 000	4,500

ies, and consequently the difference between the two ensembles is expected to be very small [30]. In addition, we have explicitly verified that no changes occur in the effective potential as the box size is increased further (i.e., ϕ_{micro} is lowered further).

In the actual calculations of the potential of mean force, ϕ_{nano} is varied from 0.0007 to 0.01, which encompasses the entire range over which stabilization is observed in the experiments. Following the experimental conditions [2,7], we choose a microsphere diameter σ_{micro}=0.6 μm and a nanoparticle diameter σ_{nano}=6 nm. Furthermore, we set Ψ_{nano} =70 mV and $\kappa\sigma_{nano}$=3.0, except when explicitly indicated otherwise. Since the colloid-nanoparticle size ratio is α =100, the resulting number of nanoparticles reaches N_{nano} =7×10^6 for ϕ_{nano}=0.007 (for ϕ_{nano}=0.01, where N_{nano} =10^7, our calculations are only accurate enough to locate the minimum in the effective potential). The corresponding computational effort is summarized in Table I.

A crucial ingredient to accelerate the simulations is the use of the cell index method with linked lists. Here, two independent sets of linked cells are employed, with cell sizes based upon the respective interaction cutoffs used. In addition, a direct mapping is used to compute the potential V_{m-n} between species that reside in different cell sets [12].

IV. RESULTS AND DISCUSSION

A. Nanoparticle adsorption

In order to investigate the validity of the interactions derived in Sec. II, we first carry out Monte Carlo simulations using the approximate expressions in Eqs. (5) and (7). The interactions are cut off at r_c^{nano}=5σ_{nano} for $V_{nano}(r)$ and r_c^{m-n} =60σ_{nano} for $V_{m-n}(r)$. Unlike in the calculations of the potential of mean force (presented below), here we wish to explicitly account for colloidal many-body effects and thus use a system containing 50 microspheres at the same volume fraction as the experiments, ϕ_{micro}=0.1. Up to 5×10^6 nanoparticles are present.

As illustrated in Fig. 1, the nanoparticle distribution $\rho_{nano}(D)$ around a microsphere (expressed as a function of the microsphere-nanoparticle surface separation D) has a very strong peak near contact, indicating the accumulation of nanoparticles around the colloids. The thickness of this ac-

cumulation layer, as determined by the minimum of $\rho_{nano}(D)$, is approximately σ_{nano}. For low volume fractions, there is only a negligible difference between the density profiles for different ϕ_{nano}. However, for higher volume fractions, ϕ_{nano} $\geq$0.001, the nanoparticle distribution starts to vary, with a more rapid decrease with increasing D and a clear minimum. By integrating $\rho_{nano}(D)$ from contact to this minimum, we compute the amount of adsorbed nanoparticles, shown in Fig. 2 along with the experimental findings [2]. As can be seen, the agreement with the experiments is fairly good. Both data sets exhibit a linear dependence on ϕ_{nano} and a degree of adsorption that is far below 100% (where every nanoparticle would be confined within the accumulation layer). The systematic overestimation in the simulations is compatible with the high nanoparticle surface potential Ψ_{nano}=70 mV [leading to contact values $V_{m-n}(D=0)=-8k_BT$ and $V_{nano}(D=0)$ =$20k_BT$], which lies somewhat above the regime of validity of the Debye-Hückel approximation employed in the HHF equation. At volume fractions above 10^{-3} the adsorption
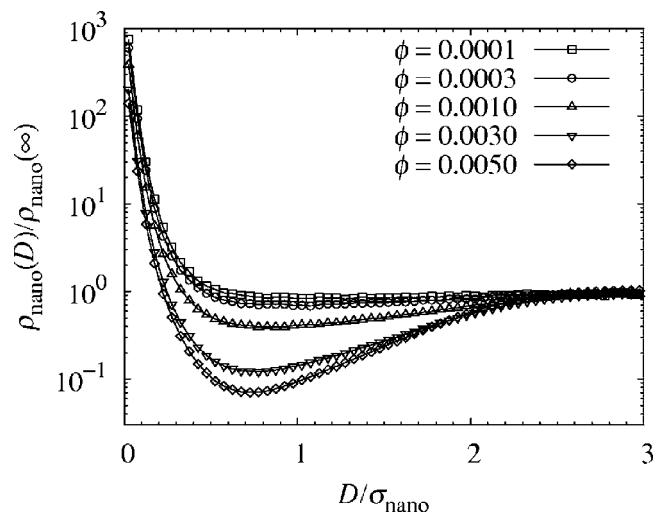

FIG. 1. Log-linear plot of the normalized density profile $\rho_{nano}(D)/\rho_{nano}(\infty)$ of nanoparticles around a microsphere as a function of the colloid-nanoparticle surface separation D, for various nanoparticle concentrations ϕ_{nano}. The accumulation near contact (D=0) results from the attractive potential. The minimum that develops with increasing ϕ_{nano} is used to define the extent of the halo.
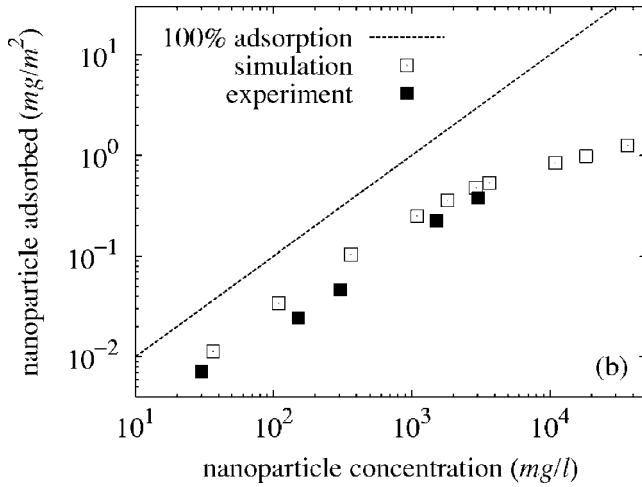
FIG. 2. Nanoparticle adsorption per colloidal microsphere as a function of nanoparticle concentration, at fixed microsphere concentration $\phi_{\text{micro}} = 0.1$. The agreement between experiment (solid squares, Ref. [2]) and simulation data (open squares) is quite reasonable, in view of the approximate potentials employed. The highest experimental concentration, 3650 mg/l, corresponds to $\phi_{\text{nano}} = 10^{-3}$.

saturates owing to mutual repulsion between the charged nanoparticles. We conclude that the pair potentials derived in Sec. II constitute a representative description of the experimental system and capture the essential interactions.

B. Effective colloidal interactions and colloidal stabilization

Since the direct interactions have been shown to provide a fairly accurate representation of the experimental system, we now proceed to calculate the resulting *effective* pair potential between the colloids, as a function of nanoparticle volume fraction ϕ_{nano}. At very low $\phi_{\text{nano}} = 7 \times 10^{-4}$ the microsphere pair correlation function [Fig. 3(a)] shows a very strong peak at a surface-to-surface distance $D = \sigma_{\text{nano}}$, corresponding to configurations in which the pair of microspheres is separated by a single nanoparticle. However, this peak is followed by a rather broad "exclusion zone," corresponding to pair separations that are extremely unlikely to occur. While the short-distance ("bridging") peak is only observed for $\phi_{\text{nano}} = 7 \times 10^{-4}$, we expect it to be present also for the other concentrations in Fig. 3(a), but the effective barrier between $D = \sigma_{\text{nano}}$ and $D \approx 2\sigma_{\text{nano}}$ makes it very unlikely for the system to arrive in such a configuration during the course of the simulation. Indeed, the potential of mean force, derived from the microsphere pair correlation function and shown in Fig. 3(b), displays a repulsive barrier of $5k_B T$ at $\phi_{\text{nano}} = 7 \times 10^{-4}$. If ϕ_{nano} is increased to 1.0×10^{-3} and 3.0×10^{-3}, the height of this barrier increases even further.

Since the van der Waals attraction between microspheres is additive to the nanoparticle-induced interaction (cf. Sec. II), it is omitted in the effective potential shown in Fig. 3(b). While it is strongly attractive at short separations, it decays rapidly with increasing microsphere separation and has a strength of approximately only $-1k_B T$ at a surface-to-surface separation $D = \sigma_{\text{nano}}$ [7]. As a result, the repulsive barrier per-

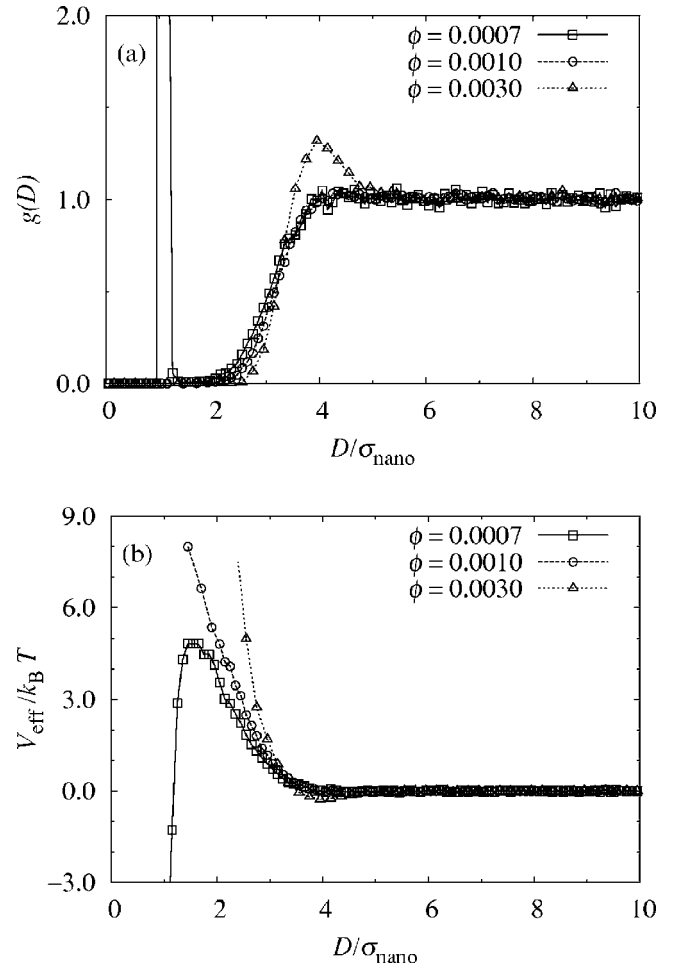FIG. 3. (a) Radial microsphere distribution function $g(D)$ as a function of surface-to-surface separation D, for nanoparticle concentrations that correspond to the stable fluid regime. (b) Corresponding effective potential $V_{\text{eff}}/k_B T$ between a pair of colloidal microspheres. At these low volume fractions, the effective interaction shows a repulsive barrier that prevents colloidal aggregation.

sists in the *net* pair interaction and is, for $\phi_{\text{nano}} \gtrsim 7 \times 10^{-4}$, sufficient to prevent gelation, resulting in kinetic stabilization of the suspension. The corresponding threshold agrees remarkably well with the experimentally observed gel-fluid transition near $\phi_{\text{nano}} = 5 \times 10^{-4}$ [2].

As foreshadowed by the local maximum in $g(D)$ for $D \approx 4\sigma_{\text{nano}}$ at $\phi_{\text{nano}} = 3.0 \times 10^{-3}$ [Fig. 3(a)], the situation changes if the nanoparticle volume fraction is raised further. The peak shifts to slightly lower separations and, more importantly, increases in height, see Fig. 4(a). This corresponds to the emergence of an effective attraction, which reaches a strength of nearly $-3k_B T$ at $\phi_{\text{nano}} = 10^{-2}$ [Fig. 4(b)]. Indeed, since this strength corresponds to the typical estimate for the onset of colloidal gelation, we identify $\phi_{\text{nano}} = 10^{-2}$ as the approximate upper bound of the stable fluid region. Again, this is in quite good agreement with the experimentally observed reentrant gelation at $\phi_{\text{nano}} \approx 5 \times 10^{-3}$, especially in view of the approximate interaction potentials employed.

A natural explanation for the reentrant behavior might be found in a depletion interaction [3] induced by the nanopar-
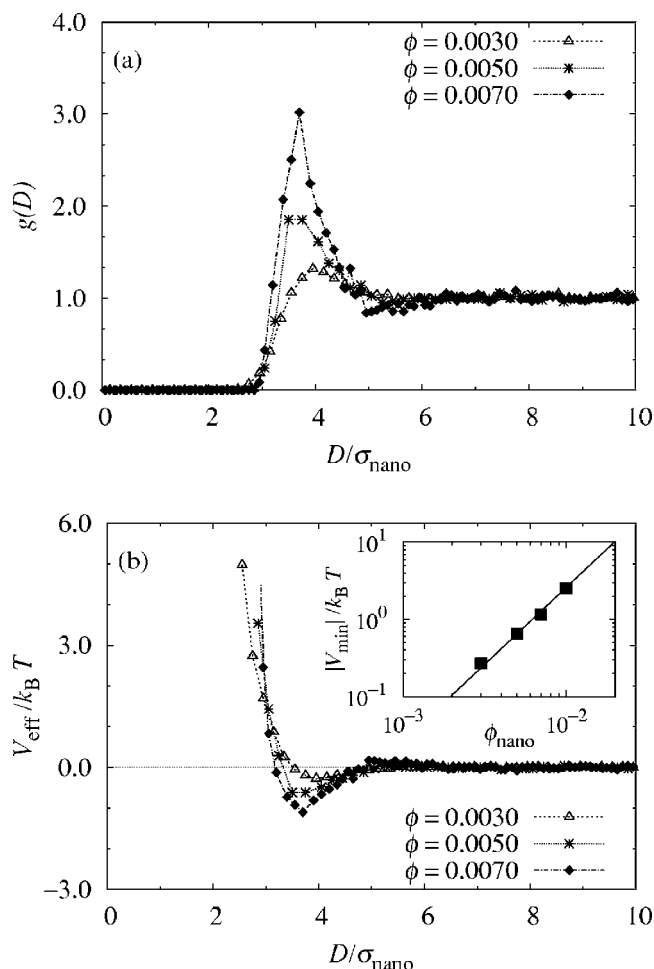
FIG. 4. Counterpart of Fig. 3, but now for higher nanoparticle volume fractions. A peak develops in the radial distribution function (a) for surface separations near $4\sigma_{\mathrm{nano}}$. The corresponding attractive minimum in the effective potential (b) grows quadratically with ϕ_{nano}, as shown in the inset. This attraction is responsible for reentrant gelation of the colloidal microspheres.

ticles, as suggested in Ref. [2]. However, as shown in the inset of Fig. 4(b), the attractive strength increases quadratically with ϕ_{nano}, whereas the classical Asakura-Oosawa (AO) theory for depletion [3] predicts an attractive minimum at contact ($D=0$), with a strength that has a linear concentration dependence. Although the quadratic dependence is observed for only less than a decade in ϕ_{nano}, and calculations for larger nanoparticle concentrations are computationally prohibitively expensive, the nonlinearity of the data appears quite pronounced. Since the attractive minimum in Fig. 4(b) does not occur at contact, one could envisage a situation in which both colloids are decorated with a layer of nanoparticles (effectively increasing the colloid diameter) and the remaining nanoparticles induce a depletion interaction. While this might account for the position of the potential minimum, it does not account for the quadratic concentration dependence, which persists even after the corresponding adjustment has been made to the nanoparticle concentration employed in the inset of Fig. 4(b). An alternative explanation for the deviation from the linear concentration dependence

might be that the strong mutual electrostatic repulsion leads to *effective* nanoparticle concentrations that considerably exceed the bare concentrations, causing the system to leave the regime of validity of the AO theory. However, even the effective concentrations are so low that no significant deviations from linearity are expected. Thus, we conclude that the effective attractions do not result from a classical depletion mechanism alone. Given the nonadditive nature of the interactions, this is not truly surprising. To support this, an examination of relevant particle configurations shows no significant nanoparticle depletion between a pair of microspheres at a separation $D \approx 4\sigma_{\mathrm{nano}}$. It appears therefore plausible that the microsphere attraction arises from correlations between the highly charged nanoparticles in the gap between the colloids.

Since an understanding of the role of size and charge asymmetry between colloids and nanoparticles is of crucial importance for potential applications, we have investigated several other parameter combinations. Employing numerical data from Ref. [31], we have been able to extend the size asymmetry to $\alpha=200$ (which involved a system with 12 $\times 10^6$ nanoparticles). Figure 5(a) displays the effective interaction resulting from a fixed nanoparticle volume fraction, $\phi_{\mathrm{nano}}=0.003$, for colloids of diameter 0.36, 0.60, and 1.20 μm (size ratio $\alpha=60$, 100, and 200, respectively). For larger σ_{micro} both the height of the repulsive barrier and the depth of the attractive minimum in the effective interaction are enhanced. This is consistent with the experimental observation [2] that both boundaries of the stable fluid region were lowered when the size of the colloidal microspheres was increased. The inset of Fig. 5(a) shows the same potentials scaled by the size asymmetry. The excellent overlap of all curves shows that the dependence on size asymmetry is almost perfectly linear. Thus, the effective interactions follow the Derjaguin approximation, according to which the force between two large, identical spheres of diameter σ can be expressed in terms of the interaction energy of two parallel plates $W(D)$ [21],

$$F^{\mathrm{Derjaguin}}(D) \approx \frac{\pi\sigma}{2}\int_D^\infty f(z)dz = \frac{\pi\sigma}{2}W(D), \qquad (8)$$

where $f(z)$ is the normal force per unit area between two flat surfaces. This relation, which is applicable to any type of force law as long as the separation D is much less than the sphere diameter σ, indeed predicts that the colloidal force (and hence the interaction potential) has a linear dependence on σ, as an increase of the colloidal diameter does not affect $W(D)$. We note that for actual colloidal stabilization not only the size ratio, but also the *absolute size* of the nanoparticles plays a role, as it determines the range of the repulsive barrier (which must exceed the range of the van der Waals interaction).

Variation of the nanoparticle charge has multiple effects, since it not only alters the nanoparticle repulsion (and hence their effective volume fraction and the halo-halo interaction), but also the formation of the halo itself through the colloid-nanoparticle attraction, Eq. (7). This is also seen by expressing the effective force between a pair colloids at surface
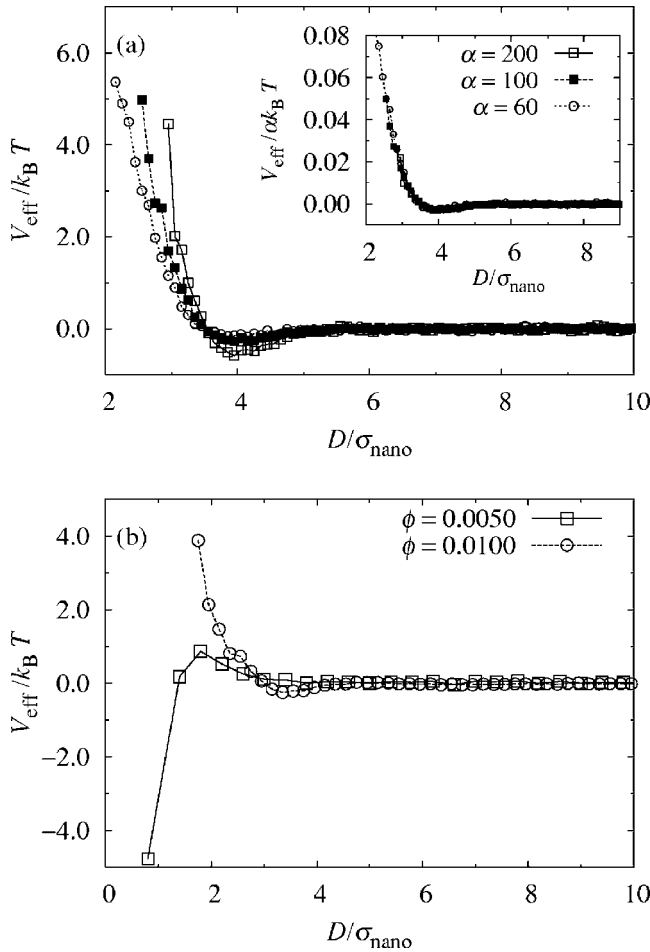
FIG. 5. (a) Effect of nanoparticle-colloid size asymmetry α on the effective colloidal interactions. At fixed nanoparticle size and volume fraction $\phi_{\text{nano}}=0.003$, both the strength of the repulsion and the depth of the attractive minimum increase with colloid size. As shown in the inset, the effective interactions show a perfectly linear scaling with α, indicating that the Derjaguin approximation applies (see text). (b) Effect of nanoparticle charge. All parameters are identical to those in Fig. 3, except for the nanoparticle surface potential, which has been lowered from 70 to 50 mV. As a result, much higher nanoparticle volume fractions are required to achieve an appreciable colloidal repulsion.

separation D in terms of the nanoparticle distribution $\rho(\mathbf{r}';D)$, where $\mathbf{r}'$ is measured with respect to the first colloid,

$$\mathbf{F}(D) = -\int \rho(\mathbf{r}';D)\frac{\partial V_{\text{m-n}}(|\mathbf{r}'|)}{\partial \mathbf{r}'}d\mathbf{r}'. \tag{9}$$

The nanoparticle charge will affect both $\rho(\mathbf{r}';D)$ and $V_{\text{m-n}}(|\mathbf{r}'|)$. Since a systematic variation of the nanoparticle charge has not been pursued in experiments, we present simulation results for the zirconia-silica system with $\alpha=100$, but at a nanoparticle surface potential that has been lowered from $\Psi_{\text{nano}}=70$ to 50 mV [see Fig. 5(b)]. The effective interactions exhibit the same trend as for higher surface potentials, but at considerably higher volume fractions. Indeed, at $\Psi_{\text{nano}}=50$ mV a given effective colloidal repulsion

is reached only at a volume fraction that is approximately ten times larger than for $\Psi_{\text{nano}}=70$ mV.

Finally, we have performed control simulations in which no attraction is present between the nanoparticles and the microspheres. Under these conditions, neither the observed nanoparticle adsorption (Fig. 2) nor the effective repulsions (Fig. 3) are recovered, except at nanoparticle concentrations that are *much* higher than in the experiment or if the nanoparticle repulsion has a much longer range than implied by the actual screening length $\kappa^{-1}\approx\sigma_{\text{nano}}/3$ [7].

C. Nanoparticle distributions

Since the effective potentials essentially result from the density distribution of the nanoparticles [cf. Eq. (9)], we have examined this distribution $\rho(\mathbf{r}';D)$ directly for a pair of colloids at fixed separation D, in order to gain insight in the origin of these potentials. Exploiting the symmetry around the z-axis passing through the centers of both colloids, we express the nanoparticle positions in cylindrical coordinates (r,ϕ,z). A rotational average is performed and the r and z coordinates of the nanoparticles are binned. For each bin, the local nanoparticle density is computed. The data shown here apply to a smaller size ratio $\alpha=40$ (i.e., $\sigma_{\text{micro}}=0.24~\mu\text{m}$), merely for reasons of clarity. The nanoparticle concentration is set to $\phi_{\text{nano}}=0.003$, resulting in a strongly repulsive effective interaction. Since the microspheres are fixed during the simulation, the conventional Metropolis Monte Carlo method is used to simulate the movement of the nanoparticles. The averages are obtained over 5000 independent samples.

At a surface separation $D=5.0\sigma_{\text{nano}}$ [Fig. 6(a)] nanoparticles accumulate in the vicinity of the colloidal surface and form a uniform, thin halo around each colloid. In this case, the effective interaction is negligibly small. If the colloids are forced closer together, the mutual repulsion between the nanoparticles leads to a redistribution of particles in the halo. At a separation $D=1.8\sigma_{\text{nano}}$ [Fig. 6(b)] most nanoparticles have been expelled from the gap region between the colloids and a depletion zone appears. While reminiscent of the depletion effect in hard-sphere mixtures [3], the effective colloidal interaction in this case is strongly *repulsive* rather than attractive. This indicates that the energy penalty resulting from nanoparticle rearrangements dominates over depletionlike entropic effects. As discussed in the context of Fig. 4(b), at a separation where a weak effective attraction is observed, namely at $D\approx4.0\sigma_{\text{nano}}$, the nanoparticle distribution looks very similar to that depicted in Fig. 6(a) for $D=5.0\sigma_{\text{nano}}$, i.e., no depletion is observed, and detection of significant differences associated with the observed attraction probably requires a spatial resolution (bin size) and statistical accuracy that exceeds what is obtained in the current work.

V. COMPARISON TO INTEGRAL-EQUATION THEORY

The system studied in this paper has also been investigated by means of integral-equation theory [13,14], in which the effective colloidal pair potential $V_{\text{micro}}^{\text{eff}}$ is computed using the two-component Ornstein-Zernike (OZ) equations supple-
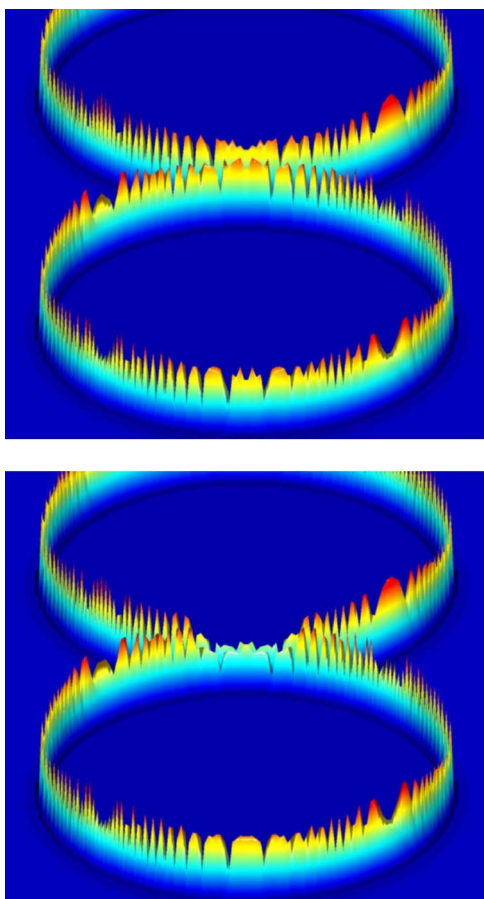
FIG. 6. (Color online) Nanoparticle density distribution around a pair of colloidal particles at a surface-to-surface distance D. (a) At larger separations ($D=5.0\sigma_{nano}$), the halos around each colloid are uniform and no appreciable effective interaction occurs. (b) Upon closer approach ($D=1.8\sigma_{nano}$), a *depletion* of nanoparticles in the gap region is observed, but the effective colloidal interaction is strongly *repulsive*, indicating that energetic terms dominate over entropic terms in the effective interaction. The jagged appearance of the distributions results from the binning procedure.

mented with the hypernetted-chain (HNC) closure. Chávez *et al.* [13] were the first to demonstrate that, under the appropriate conditions, the electrostatic repulsion between nanoparticles alone is sufficient to cause the formation of a nanoparticle monolayer on the microsphere surface. Depending on size asymmetry and nanoparticle concentration, it is also possible that the nanoparticles are less strongly bound and that a diffuse halo emerges instead of a monolayer. Rather than aiming to precisely reproduce the experimental conditions, Ref. [13] focuses on general trends. In particular, it is emphasized that, as a general criterion for the formation of a halo or monolayer, the microsphere diameter must be compared to the average (bulk) nanoparticle separation. Evidently, this criterion relies on a sufficiently strong nanoparticle repulsion. Indeed, all calculations were performed for a specific (large) choice for the screening length, $\kappa\sigma_{nano}$ $=0.15$, i.e., $\lambda\approx6.67\sigma_{nano}$. If seems doubtful that this criterion is applicable for the very different conditions of Ref. [2].

Subsequently, and coincident with the simulation results [9], another integral-equation study was performed by Ka-

ranikas and Louis [14]. They find that, for a suitable parameter choice, the effective microsphere interaction exhibits a dependence on nanoparticle concentration ϕ_{nano} that is qualitatively compatible with the experimental findings. Initially, and just as found already by Chávez *et al.* [13], the nanoparticles induce a repulsive interaction that increases in strength with nanoparticle concentration, resulting in colloidal stabilization at a concentration ϕ_{nano}^{lower}. Upon further increase of ϕ_{nano}, an attractive minimum appears in V_{micro}^{eff}, which becomes sufficiently strong to lead to reentrant gelation of the colloids at a concentration ϕ_{nano}^{upper}.

While the general trends observed in Ref. [14] are certainly encouraging, we note that there are also important quantitative discrepancies with the experimental [2] and simulational [9] findings. Various calculations in Ref. [14] employ a Debye screening length of $\lambda=5.0\sigma_{nano}$, much larger than the experimental value $\lambda\approx0.33\sigma_{nano}$ and, incidentally, rather close to the choice of Chávez *et al.* [13]. This increases the mutual repulsion between nanoparticles, to the extent where it may alter the mechanism responsible for the observed stabilization. Conversely, in Fig. 3 of Ref. [14] it is shown that for parameter choices closer to the experimental conditions (e.g., point "A" in this figure, corresponding to a screening length $\lambda=\sigma_{nano}$ and a nanoparticle contact energy $\varepsilon_{nano}=6.0k_BT$), the lower bound of the stability window is shifted to nanoparticle volume fractions that are one to two orders of magnitude larger than in Refs. [2,9], whereas the window is also considerably too narrow, $\phi_{nano}^{upper}/\phi_{nano}^{lower}\lesssim2$ instead of $\phi_{nano}^{upper}/\phi_{nano}^{lower}\approx10$. Karanikas and Louis suggest that these differences might stem from the polydisperse nature of the nanoparticles employed in the experiments. However, small-angle x-ray scattering measurements [31] have indicated that the nanoparticles, while certainly not monodisperse, have a size distribution that is considerably narrower than indicated in Ref. [2] ($2<\sigma_{nano}<4$ nm rather than $0.5<\sigma_{nano}<11$ nm). Nevertheless, these differences are not surprising because Karanikas and Louis opted not to include an explicit microsphere-nanoparticle attraction. Accordingly, halo formation can only result from nanoparticle repulsion. However, as pointed out in Ref. [9] and in Sec. I of the present paper, this mechanism is highly unlikely to be relevant under the conditions of Ref. [2], and can indeed only be made to work at either larger screening lengths or higher nanoparticle concentrations.

While, as shown above and in Ref. [9], the presence of an induced, short-range colloid-nanoparticle attraction can resolve this inconsistency, the inclusion of an attractive interaction V_{m-n} yields rather different results for the screening length chosen in the integral-equation approach [14]. If V_{m-n} and the nanoparticle repulsion V_{nano} have a comparable range, bridging attractions arise that have a detrimental effect on colloidal stability. On the other hand, if V_{m-n} is relatively long-ranged compared to V_{nano}, bridging is avoided, but also the reentrant gelation is no longer observed for the entire range of nanoparticle volume fractions investigated [14].

It is also of interest to consider instead the predictions of an integral-equation approach for the pair potentials employed in the Monte Carlo simulations [9]. Figure 7 presents a comparison between the simulation results of Figs. 3(b) and 4(b) and corresponding integral-equation results ob-
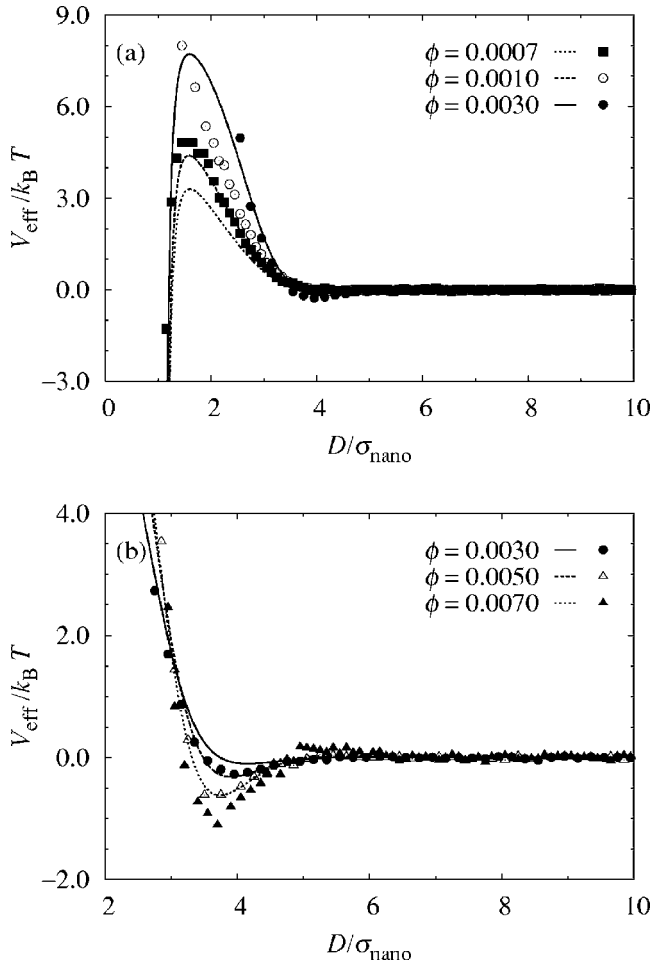
FIG. 7. Comparison of the Monte Carlo results of Figs. 3(b) and 4(b) (symbols) to HNC integral-equation results (lines) [15]. (a) At low nanoparticle volume fractions, the analytical results reproduce the nanoparticle bridging at $D = \sigma_{nano}$ as well as the repulsive barrier. Although the height of this barrier is underestimated, it increases with increasing nanoparticle concentration, as in the simulations. (b) At higher nanoparticle volume fractions, the integral-equation results reproduce the attractive minimum found in Fig. 4(b). The strength of the attraction is approximately twice smaller than in the Monte Carlo (MC) calculations.

tained using the HNC closure [15]. Despite the fact that the HNC performs best for smoothly varying potentials [32] (whereas the interactions in Sec. II vary rapidly at short separation), the integral-equation results display semiquantitative agreement with our simulation results. For low ϕ_{nano} [Fig. 7(a)], both the bridging attraction at σ_{nano} and the strong effective repulsion for larger microsphere separation are reproduced, although the height of the barrier is systematically underestimated. At $\phi_{nano} = 0.0007$ the maximum in V_{eff} is approximately 40% lower than in the MC calculations. For

higher nanoparticle concentrations [Fig. 7(b)], the secondary minimum near $D = 4.0\sigma_{nano}$ is also recovered in the HNC calculations, albeit at a weaker strength than the simulations. Overall, we view this as a significant confirmation of the results presented in Ref. [9].

VI. SUMMARY AND CONCLUSIONS

We have presented a detailed numerical study of effective interactions between micron-sized silica spheres, induced by highly charged zirconia nanoparticles. Our calculations provide an explanation for the nanoparticle haloing phenomenon discovered by Lewis and co-workers [2], reproducing both colloidal stabilization and reentrant gelation in quantitative agreement with the experimental findings. The haloing mechanism for colloidal stabilization is found to rely on rather generic features and hence may become of considerable practical importance. Our calculations provide explicit guidance for the role of charge and size asymmetry between the colloids and the nanoparticles. The presence of weak colloid-nanoparticle attractions is found to be a crucial ingredient for stabilization at the very low nanoparticle volume fractions and strong screening conditions in the experiments. It is possible that the microsphere-nanoparticle interaction employed in our calculations is only an effective representation of the actual attraction, which in fact may have several different origins. However, our potentials model the experimental system fairly accurately, as shown by comparison to the experimental adsorption data, and the central result of the present work is the resulting explanation of a window of stability in the phase diagram. Integral-equation calculations using the hypernetted-chain closure have provided a semiquantitative confirmation of the effective interactions computed in the Monte Carlo simulations. We note the simulations involve not only large size asymmetries, but also extremely large numbers of particles. The use of a geometric Monte Carlo algorithm [10–12] was therefore indispensable.

[1] R. J. Hunter, *Foundations of Colloid Science*, 2nd ed. (Oxford University Press, Oxford, 2001).

[2] V. Tohver, J. E. Smay, A. Braem, P. V. Braun, and J. A. Lewis, Proc. Natl. Acad. Sci. U.S.A. **98**, 8950 (2001).

[3] S. Asakura and F. Oosawa, J. Chem. Phys. **22**, 1255 (1954).

[4] J. M. Méndez-Alcaraz and R. Klein, Phys. Rev. E **61**, 4095 (2000).

[5] R. Roth, R. Evans, and A. A. Louis, Phys. Rev. E **64**, 051202 (2001).

[6] A. A. Louis, E. Allahyarov, H. Löwen, and R. Roth, Phys. Rev. E **65**, 061407 (2002).

[7] V. Tohver, A. Chan, O. Sakurada, and J. A. Lewis, Langmuir **17**, 8414 (2001).

[8] Note that "nonadditivity" here refers to the cross diameter of the microspheres and the nanoparticles, which, in the presence of additional interactions, is not equal to the sum of their hard-sphere radii.

[9] J. Liu and E. Luijten, Phys. Rev. Lett. **93**, 247802 (2004).

[10] C. Dress and W. Krauth, J. Phys. A **28**, L597 (1995).

[11] J. Liu and E. Luijten, Phys. Rev. Lett. **92**, 035504 (2004).

[12] J. Liu and E. Luijten, Phys. Rev. E **71**, 066701 (2005).

[13] M. Chávez-Páez, P. González-Mozuelos, M. Medina-Noyola, and J. Méndez-Alcaraz, Physica A **341**, 1 (2004).

[14] S. Karanikas and A. A. Louis, Phys. Rev. Lett. **93**, 248303 (2004).

[15] S. Karanikas and A. A. Louis (unpublished).

[16] W. B. Russell, D. A. Saville, and W. R. Schowalter, *Colloidal Dispersions* (Cambridge University Press, Cambridge, U. K., 1989).

[17] T. L. Hill, *Statistical Mechanics: Principles and Selected Applications* (McGraw-Hill, New York, 1956).

[18] M. Dijkstra, R. van Roij, and R. Evans, Phys. Rev. E **59**, 5744 (1999).

[19] E. J. Verwey and J. T. G. Overbeek, *Theory of the Stability of Lyophobic Colloids* (Elsevier, Amsterdam, 1948).

[20] R. Hogg, T. W. Healy, and D. W. Fuerstenau, Trans. Faraday Soc. **62**, 1638 (1966).

[21] J. N. Israelachvili, *Intermolecular and Surface Forces*, 2nd ed. (Academic, San Diego, 1992).

[22] V. A. Parsegian and D. Gingell, Biophys. J. **12**, 1192 (1972).

[23] J. E. Sader, S. L. Carnie, and D. Y. C. Chan, J. Colloid Interface Sci. **171**, 46 (1995).

[24] L. Belloni and O. Spalla, J. Chem. Phys. **107**, 465 (1997).

[25] S. H. Behrens and M. Borkovec, Phys. Rev. E **60**, 7040 (1999).

[26] P. M. Biesheuvel, J. Colloid Interface Sci. **275**, 514 (2004).

[27] J. G. Malherbe and S. Amokrane, Mol. Phys. **97**, 677 (1999).

[28] R. Dickman, P. Attard, and V. Simonian, J. Chem. Phys. **107**, 205 (1997).

[29] E. Allahyarov, I. D'Amico, and H. Löwen, Phys. Rev. Lett. **81**, 1334 (1998).

[30] J. Wu, D. Bratko, and J. M. Prausnitz, Proc. Natl. Acad. Sci. U.S.A. **95**, 15169 (1998).

[31] C. J. Martinez, J. Liu, S. K. Rhodes, E. Luijten, E. R. Weeks, and J. A. Lewis, Langmuir **21**, 9978 (2005).

[32] J.-P. Hansen and I. R. McDonald, *Theory of Simple Liquids*, 2nd ed. (Academic, San Diego, 1986).